Molecular Aggregation and Luminescence Properties of Bulk Poly(2,5-di-*n*-octyloxy-1,4-phenylenevinylene)

S. H. Chen, A. C. Su,* and S. R. Han

Institute of Materials Science and Engineering, National Sun Yat-sen University, Kaohsiung 804, Taiwan

S. A. Chen and Y. Z. Lee

Department of Chemical Engineering, National Tsing Hua University, Hsinchu 300, Taiwan

Received August 19, 2003; Revised Manuscript Received November 5, 2003

ABSTRACT: Structural development in cast films of poly(2,5-di-*n*-octyloxy-1,4-phenylenevinylene) (DO-PPV) upon heat treatment was studied by means of polarized light microscopy, X-ray diffraction, ultraviolet−visible spectroscopy, and photoluminescence spectroscopy as well as scanning and transmission electron microscopy. Results indicated the dominance of a lamellar phase of biaxially refringent nematic-like texture upon short-term heat treatments at elevated temperatures (T_a) between 160 and 240 °C. A further increase in T_a results in dissipation of the mesomorphic order near the isotropization temperature T_i = ca. 300 °C. This lamellar phase, 1.8 nm in layer spacing at room temperature, typically consists of beads or grains approximately 10−20 nm in diameter that agglomerate into wormlike features in the absence of external stress. Mechanical shear right after high-temperature annealing results in disintegration of worms formed in the tranquil state; the constituent beads nevertheless reagglomerate into new wormlike entities whose long axes lie perpendicular to the shear direction, with the DO-PPV backbones and the lamellae lying parallel to the shear direction. The optical absorption edge at 590 nm and the photoexcited emissions at 600 and 630 nm remained independent of structural development at low to intermediate T_a's; however, structural dissipation near T_i results in a clear shift of absorption edge to 570 nm whereas the emission maximum blue-shifted to 585 nm. In combination of transient absorption and emission spectra during cooling of a dilute DO-PPV/*p*-xylene solution as well as published results of time-resolved emission studies, we conclude that the emission at 585 nm corresponds to signle chromophores in disordered DO-PPV chains, whereas the emissions at 600 and 630 nm correspond respectively to single chromophores of extended conjugation and excimer-like interchain species within the ordered lamellar domains.

Introduction

Poly[2-methoxy-5-(2′- ethylhexyloxy)-1,4-phenylenevinylene] (MEH-PPV) is one of the most extensively studied electroluminescent (EL) polymers.[1] The concept behind the molecular design of MEH-PPV is the use of asymmetric substitutions of methyloxyl and branched ethylhexyloxyl side chains to improve solubility in common solvents and suppress molecular aggregation.[2] Nevertheless, there still exists significant tendency toward molecular aggregation, which in turn gives rise to strong morphological effects on its light emission properties.[3−10] By means of X-ray diffraction (XRD) and transmission electron microscopy (TEM), we have recently shown unequivocally for MEH-PPV the presence of molecular aggregation via formation of a biaxial nematic mesophase of sanidic nature, which is accompanied by a clear red shift of emission maximum from 590 to 640 nm.[11,12] The practical significance of such fundamental understanding in morphology effects is most clearly demonstrated by a recent study[13] on changes in emission wavelengths upon heat treatment (although in a more limited temperature range) and improved EL efficiencies attributable to more balanced electron/hole transport.

One possible explanation for the observed molecular aggregation is that the methoxyl substituent is too short to provide adequate shielding of the backbone to avoid interbackbone contacts in MEH-PPV. This is based on the idea that the formation of aggregates is driven mainly by the aromatic−aromatic attraction between backbones. On the other hand, as previously proposed for hairy-rod polymers in general, molecular aggregation may simply be a result of incompatibility between the flexible (aliphatic) side chains and the semirigid (aromatic) backbones, reminiscent of comb-shaped block copolymers and side-chain liquid crystalline polymers.[14] In better agreement with this latter expectation, Fann et al.[15−18] have previously proposed that significant intermolecular aggregation occurs in the case of poly(2,5-di-*n*-octyloxy-1,4-phenylenevinylene) (DO-PPV), a close homologue of MEH-PPV but with comparatively long and linear side-chain substitutions. As these studies were mainly based on time-resolved photoluminescence spectroscopic observations, we feel that direct evidences of aggregate formation, with the relevant morphological characteristics clarified, would be more helpful in the understanding of molecular aggregation in semiconducting polymers in general.

Here we present results of our recent morphological study of bulk DO-PPV. We show that molecular aggregation indeed occurs in DO-PPV via formation of a lamellar mesophase with interlayer spacing of ca. 1.8 nm, in support of the idea that it is generally the amphiphilicity (van der Waals interactions between aliphatic side chains and those between aromatic backbones) that are responsible for supramolecular self-assembly of hairy-rod polymers. We show also that the

* Corresponding author: e-mail acsu@mail.nsysu.edu.tw.

10.1021/ma035230n CCC: $27.50
Published on Web 12/13/2003

formation of the mesomorphic order bears significant effects on optical absorption and emission properties.

Experimental Section

Poly(2,5-di-*n*-octyloxy-1,4-phenylenevinylene) (DO-PPV, chemical structure given as inset in Figure 7a) material was synthesized from 2,5-di-*n*-octyloxy-1,4-bis(bromomethyl)benzene via the Gilch method, following in general the procedure reported by Wudl et al.[19] Weight-average molecular mass determined by means of gel permeation chromatography using polystyrene standards was 2 MDa, with polydispersity index of 5. The carrier solvent was tetrahydrofuran, which is a fair solvent for DO-PPV at room temperature as compared to toluene or *p*-xylene used in our morphological studies. Although a standard prefiltration procedure was adopted, the possible existence of minor aggregates cannot be excluded; the given values of molecular mass and polydispersity should therefore be regarded as upper bounds.

Polarized light microscopic (PLM) observations were made by use of a Nikon Eclipse E400-POL microscope equipped with a temperature-controlled stage. A Siemens D5000 diffractometer equipped with a copper target (Kα line, 0.154 nm in wavelength) and a graphite collimator to obtain 1-D ("powder") X-ray diffraction (XRD) profiles under a step-scan rate of 0.05° per 3 s in the scattering angle range of $2\theta = 1°-41°$. Transmission electron microscopic (TEM) studies were performed using a JEOL 3010 instrument under an acceleration voltage of 200 kV, at which the combined factor of wavelength and camera length has been carefully calibrated using (111), (200), (220), and (311) reflections from vapor-deposited Al thin film. Surface topographic features were examined via secondary electron images (SEI) obtained by use of a field-emission scanning electron microscope (JEOL JSM-6330TF) under an accelerating voltage of 10 kV. Optical absorption (UV−vis) and photoluminescence (PL) spectra of the film specimens were obtained by use of a Hong-Ming MFS-230 instrument. In the case of transient spectroscopic UV−vis/PL measurements on a dilute (i.e., 15 ppm) DO-PPV solution in *p*-xylene during natural cooling, the solution temperature and the elapsed time were simultaneously recorded by use of a thermocouple immersed in the sample cell and a stopwatch, respectively. In obtaining the PL spectra, the excitation wavelength is fixed at $\lambda_{ex} = 450$ nm for the sake of consistency between film and solution studies. This wavelength is slightly to the blue side of the main absorption peak centering around 460−500 nm so that proper excitation of all relevant chromopohores is ensured. Additional experiments indicated that varying λ_{ex} from 450 to 490 nm bears little effects on the obtained PL spectra though.

Film specimens were drop-cast from toluene solutions (typically 0.2 wt % for PLM and XRD experiments and less than 0.1 wt % for TEM specimens, prepared via warming the solutions in a hot water bath to ca. 80 °C for 5 min) on quartz or glass substrate. Routine drying (4 h at 80 °C under vacuum) and heat treatment (5 min at an elevated temperature under a protective stream of nitrogen, followed by fast cooling to room temperature) procedures were typically adopted to follow the thermally induced structural change or its effects on absorption/emission behavior. Oriented films were obtained via manual shearing at 230 °C, followed by fast cooling to room temperature. For TEM studies, specimens were detached from the substrate using aqueous HF solutions and vacuum-deposited with carbon.

Molecular simulation of single-chain conformation was performed by means of the Cerius2 software on a Silicon Graphics workstation, with energy minimization achieved via iterated calculations on the basis of the Universal 1.01 all-atom force field.

Results and Discussion

Phase Behavior. Given in Figure 1 are optical micrographs of a drop-cast specimen. The as-cast film was only weakly birefringent under cross-polarization.

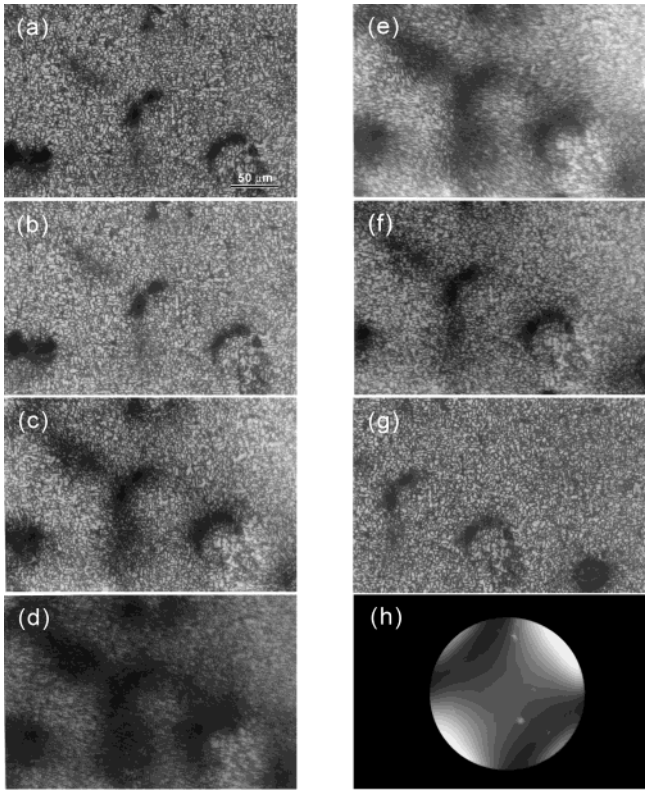

Figure 1. Cross-polarized optical micrographs of DO-PPV during a thermal cycle between room temperature and 290 °C at a heating/cooling rate of 20 °C/min: (a) at room temperature after cooling from a preliminary heating to 260 °C, (b) reheated to 140 °C, (c) heated to 250 °C, (d) heated to 260 °C, (e) cooled from 290 to 245 °C, (f) cooled to 230 °C and (g) room temperature with optical texture fully recovered, and (h) conoscopic interference pattern of an oriented specimen, suggesting biaxial birefringence.

Nematic-like optical texture became more apparent upon cooling from a transient increase in temperature (cf. Figure 1a). During the subsequent thermal cycling between room temperature and 290 °C at a heating/cooling rate of 20 °C/min, there exists gradual thermochromic changes (from orange to green) up to 200 °C, but little variation in the Schlieren texture (cf. Figure 1b,c). The birefringence weakens above 260 °C, with some fluidlike flow as indicated by the slightly smeared appearance of Figure 1d. The optical texture is reversibly recovered upon cooling from 290 °C (Figure 1e−g). The conoscopic interference pattern for an oriented specimen (sheared at 230 °C, followed by fast cooling) suggests optical biaxiality (cf. Figure 1h).

Given in Figure 2 are XRD profiles of a film specimen obtained upon fast cooling to the ambient condition from a short-term (i.e., 5 min) heat treatment at an elevated temperature (T_a). The thermal history was design in such a way that the isothermal treatments were made at a sequence of increasingly higher temperatures. For the as-cast film, there already exist some minor ordering as indicated by the presence of a weak peak near $2\theta = 4.8°$ in the XRD profile, which translates to a *d* spacing value of 1.8 nm. During the subsequent 4 h vacuum-drying at 80 °C, another transient structure is developed (without apparent perturbation of the existing order within as-cast film), showing as a broad peak around $2\theta = 2.9°$, which corresponds to a *d* spacing value of 3.0 nm. With the dissipation of this transient structure upon the subsequent heat treatment at $T_a = 120$ °C,

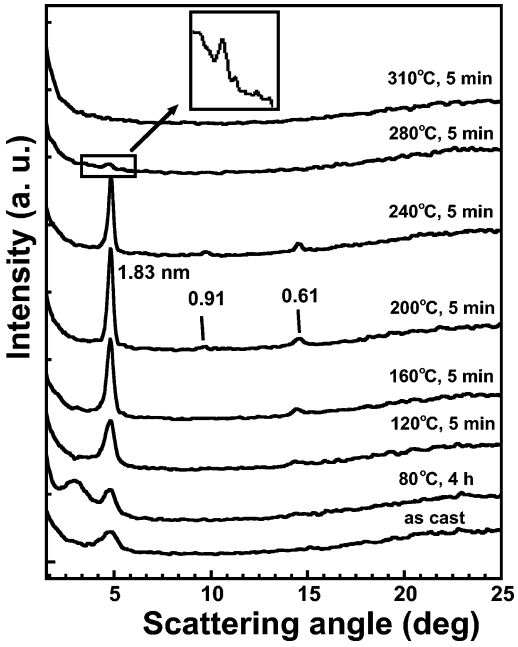

Figure 2. Room temperature XRD profiles of a film specimen obtained during a sequence of heat treatments at increasingly higher temperatures. The heat treatment temperature and the elapsed time at this temperature are as indicated for each curve.

the intensity of the preexisting peak is clearly increased. Subsequent heat treatments at $T_a = 160-240$ °C result in better development of this peak as well as its second- and third-order reflections, suggesting lamellar structure for this mesomorphic phase. At a higher T_a of 280 °C, all three reflections are weakened, indicating dissipation of the lamellar order; completion of the disordering process is achieved only as T_a is further increased to 310 °C. In combination with our PLM results, these XRD observations indicate the dominance of a liquid crystalline phase with the isotropization temperature T_i = ca. 300 °C.

Structural Features. Given in Figure 3a is a representative TEM bright field image for thin specimens annealed at T_a of 250 °C, where the lamellar mesophase is fully developed as judged from XRD results. The most prominent morphological feature here is the abundance of wormlike entities approximately 200 nm in length and 10−20 nm in width. A closer examination indicates that each of these worms is composed of a string of beads 10−20 nm in size, as confirmed by the surface topographic features shown in Figure 3b. At a lower T_a of 200 °C, the beads appear even better connected to give necklaces exceeding micrometers in length (cf. Figure 4a,b).

It is then interesting to observe from the bright field image (cf. Figure 5a) that shear orientation immediately after structural development results in disintegration of the worms or the necklaces, but the beads nevertheless reagglomerate into wormlike entities with the long axes lying approximately perpendicular to the shear direction. The corresponding selected-area electron diffraction (SAED) pattern in Figure 5b indicates that the backbones are indeed aligned in the shear direction as the meridional arc (0.63 nm in *d* spacing) corresponds to monomeric repeat along the backbone in the fully extended conformation according to results of molecular mechanics calculations over DO-PPV single chain. Three of the equatorial arcs, 1.84, 0.92, and 0.61 nm in *d* spacing, may respectively be assigned to the lamellar periodicity and the corresponding second- and third-order reflections. This indicates that the layers are also

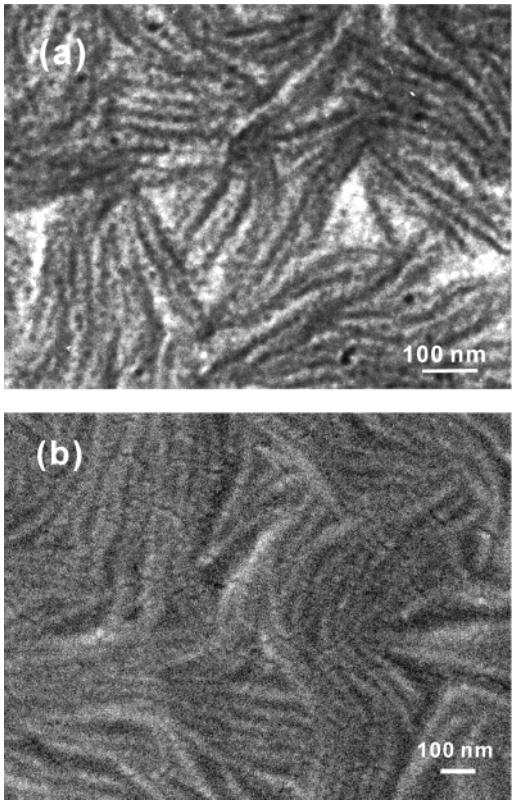

Figure 3. (a) TEM bright-field image and (b) SEM secondary electron image obtained from specimen annealed at 250 °C for 1 min followed by fast cooling to room temperature.

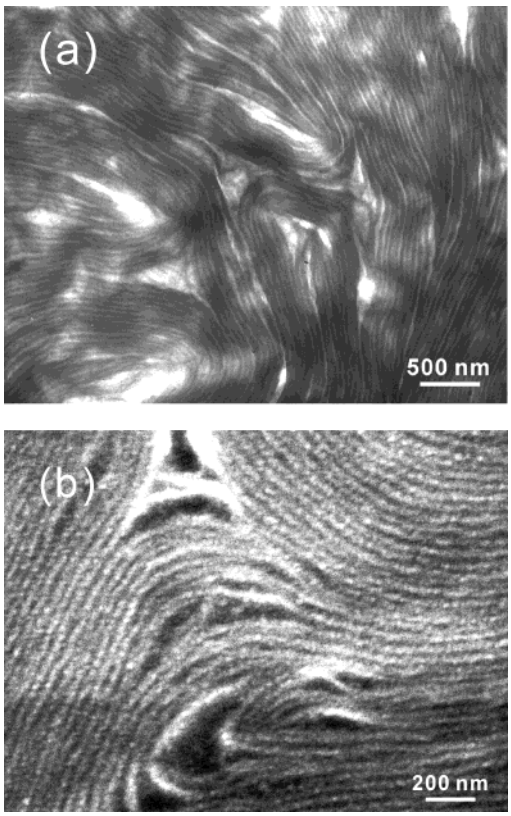

Figure 4. (a) TEM bright-field image and (b) SEM secondary electron image obtained from specimen annealed at 200 °C for 5 min followed by fast cooling to room temperature.

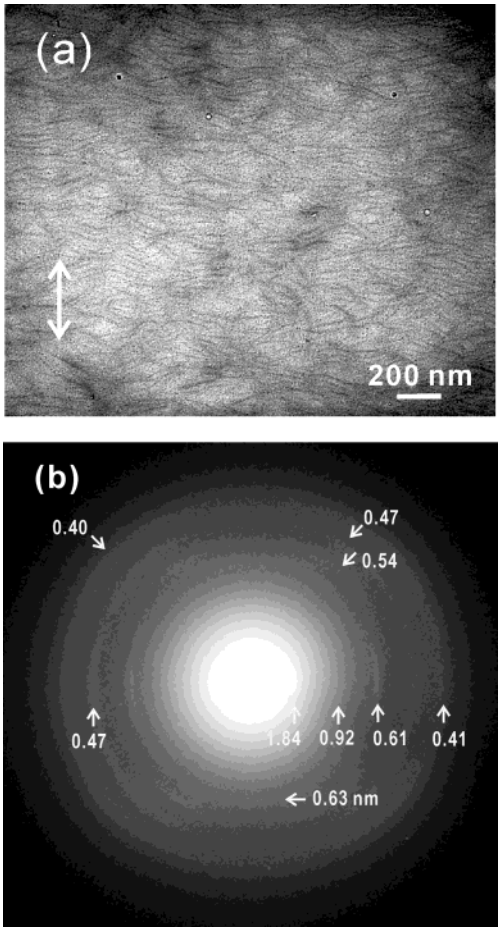

Figure 5. (a) TEM bright field image (with shear direction indicated by two-way arrows) and (b) the corresponding SAED pattern (with shear direction along the meridian) for specimen sheared (after 5 min annealing) at 230 °C.

aligned in the shear direction, with the layer normal lying parallel to the long axis of the worm. Therefore, we conclude that the wormlike entities in the sheared specimen are composed of transversely reagglomerated beads, within which the DO-PPV backbones are aligned in the shear direction. Note that this picture is consistent with the optical biaxiality implied in Figure 1h.

The remaining equatorial arc of 0.47 nm in *d* spacing may be attributed to interbackbone spacing within each boardlike sublayer composed of aligned DO-PPV backbones. The three off-axis arcs (with *d* spacing values of 0.54, 0.47, and 0.40 nm) indicate some additional order within the lamellar structure. There is a long and relatively broad arc (0.41 nm in *d* spacing) for azimuthal angles above 30°, partly overlapping with the off-axis arc of 0.40 nm in *d* spacing. This corresponds to the strongest diffraction peak of polyethylene (i.e., the characteristic (110) reflection in both the orthorhombic and the monoclinic forms)[20] and is attributed to the reflection from locally parallel packing of alkyl side chains. The diffuse nature and the broad span in azimuthal angle indicate rather localized development of order and absence of orientation preference. The (idealized) transverse span of a DO-PPV chain with fully extended side chains would be 2.68 nm; compared to the experimental layer spacing of 1.84 nm, the alkyl side chains must on average tilt from the backbone by ca. 47°. A naive picture of herringbone arrangement of fully extended side chains, however, is certainly oversimplified in view of the wide spread in azimuthal angle but may still serve as a first approximation to the mode of molecular packing.

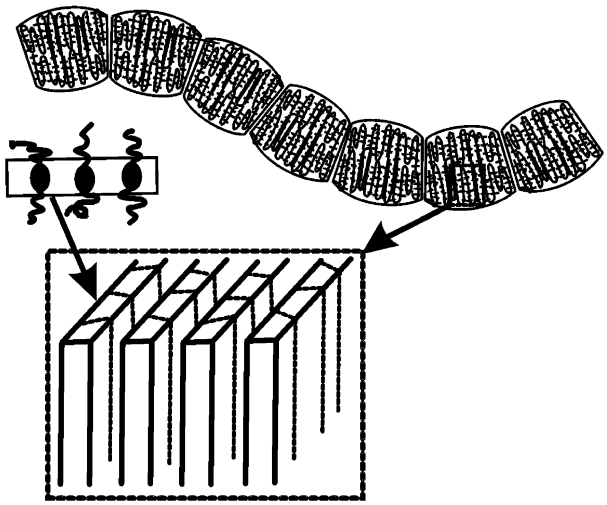

Figure 6. Schematic presentation of hierarchical features of DO-PPV aggregates.

Morphological Model. Given in Figure 6 is a schematic model connecting the lamellar mesophase in the molecular level to agglomerated wormlike morphology observed in the electron micrographs shown in Figures 3−5. In this model, each bead (approximately 10−20 nm in size, with truncated flat ends) is composed of boardlike entities formed by aggregated DO-PPV backbones. The beads, in turn, are weakly attached side-by-side in the transverse direction to give wormlike features. It follows that, upon shear at an elevated temperature, the "worms" are disintegrated into units of beads, within which the DO-PPV backbones and the lamellar assemblies are aligned in the shear direction; the beads subsequently reagglomerate into new wormlike entities whose long axes lie perpendicular to the shear direction, with the DO-PPV backbones and the lamellae lying parallel to the shear direction. This is similar to the model[12] we previously proposed for the sanidic mesophase of MEH-PPV, except that the boardlike entities of aggregated backbones are evenly spaced to account for the development of lamellar order.

Optical Absorption/Emission Properties. Shown in Figure 7 are optical absorption and photoexcited emission spectra of a film specimen subjected to the same thermal history as that given in Figure 2. In the as-cast state or after heat treatment at T_a up to 240 °C, there are no significant changes in the absorption spectra, which are characterized by a maximum absorption near 490 nm and an absorption edge near 590 nm. There are also no discernible differences in the corresponding emission spectra (excited at $\lambda_{ex} = 450$ nm), which are characterized by emissions at 600 and 630 nm of similar intensities. The energy difference between these two wavelengths is 800 cm^{-1}, much lower than the expected phonon gap (1310 cm^{-1})[21] for the phenylenevinylene backbone; therefore, these two emission peaks are not associated through phonon coupling and should be of different photophysical origins.

As structural order is dissipated upon heat treatment at $T_a = 280$ °C, the absorption maximum is blue-shifted to ca. 480 nm and the absorption edge to 580 nm. In the meanwhile, the emission spectra show significant changes in that the short-wavelength emission is slightly blue-shifted to 593 nm and that the high-wavelength

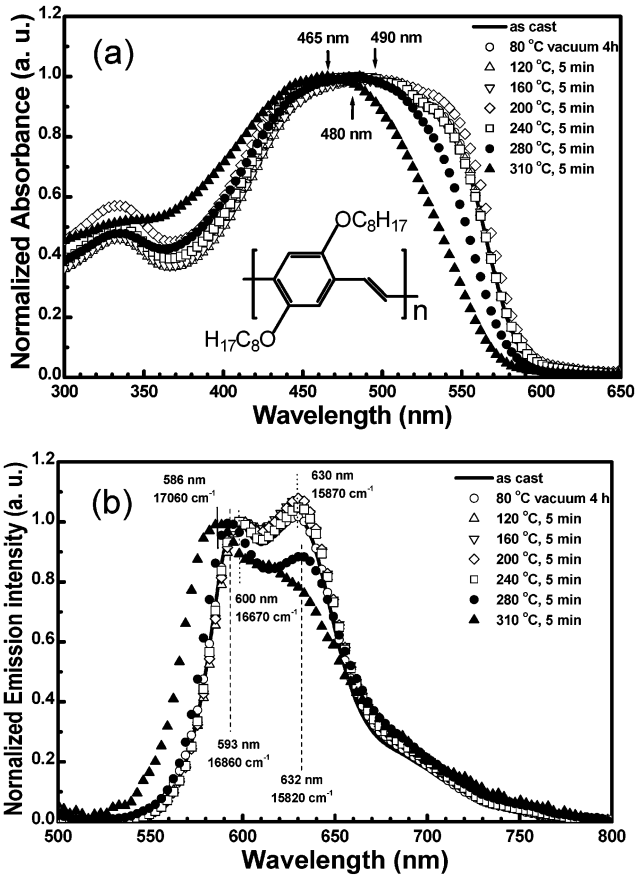

Figure 7. Variations of (a) absorption and (b) photoexcited (λ_{ex} = 450 nm) emission spectra of DO-PPV film specimen during a sequence of cumulative isothermal treatments at increasingly higher temperatures. Note that the thermal history coincides exactly with that of the XRD study (cf. Figure 2).

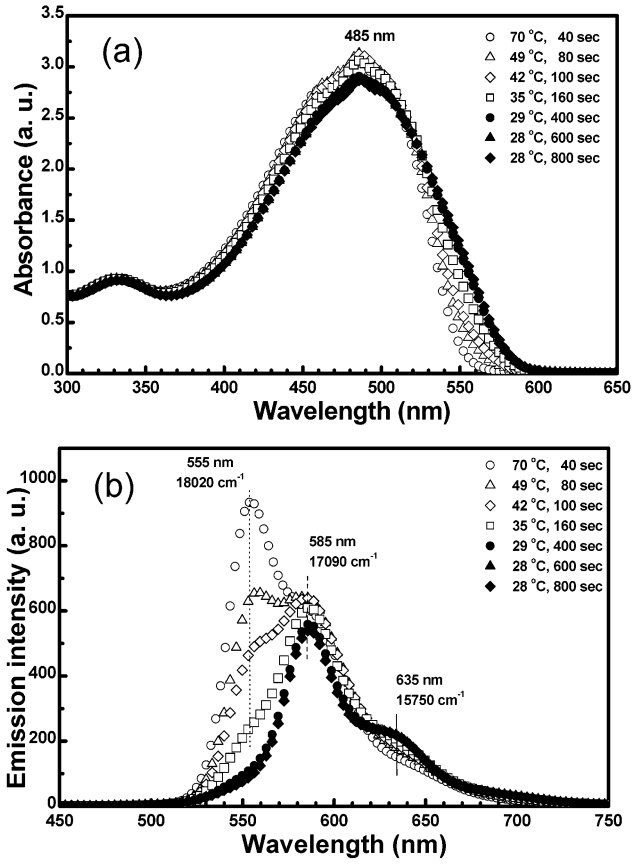

Figure 8. Variations of (a) absorption and (b) photoexcited (λ_{ex} = 450 nm) emission spectra of a dilute (15 ppm) solution of DO-PPV in *p*-xylene during natural cooling from ca. 80 °C. The elapsed time and the corresponding temperature are as indicated.

emission is red-shifted slightly to 632 nm, with a clear decrease in relative intensity. Complete elimination of structural order upon heat treatment at T_a = 310 °C results in further blue shifts in absorption maximum to 465 nm and absorption edge to ca. 570 nm. Correspondingly, the emission spectrum becomes dominated by a further blue-shifted emission at 587 nm, whereas the emission intensity at 632 nm is further decreased to become a shoulder; the energy difference between the two wavelengths is now 1240 cm^{-1}, in better agreement with the expected phonon gap.

For clarification of origins of the two main emissions, we present in Figure 8 absorption and emission spectra of a dilute (i.e., 15 ppm) solution of DO-PPV in *p*-xylene. In this extremely diluted case, complete dissolution of DO-PPV is at least apparently achieved upon warming to ca. 80 °C. The absorption spectra are characterized by the absorption maximum near 485 nm that is little affected by the decrease in temperature, but the absorption edge is clearly red-shifted from 550 to 580 nm upon cooling. There are, however, more dramatic changes in the emission spectrum. When the solution is hot, the emission spectrum is composed of a main emission at 555 nm and a shoulder at 585 nm. The small energy difference of 940 cm^{-1} rules out the possibility of phonon coupling between the two emissions. Upon standing (and natural cooling) in the spectrometer, the emission at 555 nm decreases quickly with decreasing temperature whereas the intensity of the "shoulder" at 585 nm remains unaltered. (Note that the intensity readings given here are absolute values without normalization.) As the temperature reaches 42 °C, the intensity of the emission at 555 nm becomes weaker than that of the emission at 585 nm whereas a third peak at 635 nm starts to emerge. When the solution is brought closer to the ambient temperature upon further standing, the short-wavelength emission at 555 nm diminishes entirely whereas intensities of the two long-wavelength emissions at 585 and 635 nm remain largely unaltered.

The emission at 555 nm is readily attributable to single-chromophore emission of molecularly dissolved DO-PPV chains, as its intensity decreases clearly with the decrease in solvency power via a lowering in temperature. The emission at 585 nm may therefore be attributed to aggregated DO-PPV chains. (Dynamic light scattering measurements at room temperature indeed indicated the presence of particles ca. 300 nm in size for a 100 ppm solution in toluene that is of similar solvency power as *p*-xylene. The particle size is expected to decrease upon further dilutions, but the signals drop below our instrumental detection limit.) It is tempting to assign the emission at 635 nm to a phonon sideband of the emission at 585 nm, as the energy difference between the two is 1340 cm^{-1}. However, the strong decrease in quantum yield upon respective disappearance and emergence of emissions at 555 and 635 nm suggests that the latter emission is of very low PL efficiency and hence unlikely a phonon sideband of the peak at 585 nm that remains largely unaffected during the entire process. We therefore conclude that the emission at 635 nm is more likely the excimer emission from aggregated DO-PPV chains.

With these interpretations in mind, we return to the emission behavior of the film specimen shown in Figure 7b. The emission at 585 nm upon complete dissipation of lamellar order may now be attributed to single-chromophore emission of DO-PPV chains packed in a disordered manner. Formation of the lamellar mesophase must have resulted in extended conjugation as to give red-shifted emission at 600 nm. This attribution of increased conjugation length upon ordering is supported by the observation of continuous shifts of emission maximum from 600 to 585 nm upon gradual disruption of the lamellar order (cf. Figure 7b). The emission at 630 nm must therefore involve interchain species (as indicated previously by Fann et al.[15−18] on the basis of photophysical evidence) that are very likely excimers in view of results from our dilute solution study.

The present study focuses on the "morphology effect": all spectroscopic measurements on DO-PPV films were made at room temperature and hence represent effects for changes in molecular packing at room temperature *after* short-term annealing at elevated temperatures. This is not to be confused with thermochromic effects often attributable to changes in conjugation length with varying temperature in the absence of morphological changes. As a final note, we also wish to add that possible interferences from photo- or thermo-oxidation of DO-PPV during the present short-term heat-treatment procedure have been excluded in view of previous infrared spectroscopic evidence[12] in the case of its closely related homologue, MEH-PPV.

Conclusion

The present results clearly indicate the formation of a lamellar mesophase in bulk DO-PPV, in contrast to the biaxial nematicity[12] previously observed in bulk MEH-PPV. Similar to MEH-PPV, the backbones of DO-PPV are fully extended (or nearly so) and transversely stacked to give boardlike characteristics; the symmetrically grafted linear side chains of longer length in the present case render the boards more evenly spaced though. The fact that longer side chains of DP-PPV result in a better ordered mesophase lends support to the concept that it is generally the amphiphilicity (i.e., van der Waals interactions between aliphatic side chains and those between aromatic backbones) that are responsible for supramolecular self-assembly of hairy-rod polymers. Also reported are novel observations of a hierarchy of morphological features built from nanograins of lamellar mesophase. Photoexcited emissions from DO-PPV films at 600 and 630 nm are attributed to single-chromophore excitons of extended conjugation and excimer excitons, respectively, upon ordered packing of DO-PPV chains in the lamellar mesophase; the emission at 585 nm is attributed to single-chromophore excitons in DO-PPV chains packed in a disordered manner.

Acknowledgment. This work is financially supported in part by the Ministry of Education under Contract 91E-FA04-2-4A and in part by the National Science Council under Contract NSC91-2216-E-110-007. Thanks are also due to H. L. Chou and Y. H. Lee at IMSE, NSYSU, for molecular simulation and dynamic light scattering measurements.

References and Notes

(1) Friends, R. H.; Gymer, R. W.; Holmes, A. B.; Burroughes, J. H.; Marks, R. N.; Taliani, C.; Bradley, D. D. C.; dos Santos, D. A.; Gredas, J. L.; Loglund, M.; Salaneck, W. R. *Nature (London)* **1999**, *397*, 121.
(2) Kraft, A.; Grimsdale, A. C.; Holmes, A. B. *Angew. Chem., Int. Ed.* **1998**, *37*, 402.
(3) Nguyen, T. Q.; Doan, V.; Schwartz, B. J. *J. Chem. Phys.* **1999**, *110*, 4068.
(4) Shi, Y.; Liu, J.; Yang, Y. *J. Appl. Phys.* **2000**, *87*, 4254.
(5) Nguyen, T. Q.; Martini, I. B.; Liu, J.; Schwartz, B. J. *J. Phys. Chem. B* **2000**, *104*, 237.
(6) Lee, T. W.; Park, O. O. *Adv. Mater.* **2000**, *12*, 801.
(7) Liu, J.; Shi, Y.; Ma, L.; Yang, Y. *J. Appl. Phys.* **2001**, *88*, 605.
(8) Nguyen, T. Q.; Schwartz, B. J.; Schaller, R. D.; Johnson, J. C.; Lee, L. F.; Haber, L. H.; Saykally, R. J. *J. Phys. Chem. B* **2001**, *105*, 5153.
(9) Tan, C. T.; Inigo, A. R.; Fann, W. S.; Wei, P. K.; Perng, G. Y.; Chen, S. A. *Org. Electron.* **2002**, *3*, 81.
(10) Collison, C. J.; Rothberg, L. J.; Treemaneekarn, V.; Li, Y. *Macromolecules* **2001**, *34*, 2346.
(11) Chen, S. H.; Su, A. C.; Huang, Y. F.; Su, C. H.; Peng, G. Y.; Chen, S. A. *Macromolecules* **2002**, *35*, 4229.
(12) Chen, S. H.; Su, A. C.; Chou, H. L.; Han, S. R.; Peng, K. Y.; Chen, S. A. *Macromolecules*, in press.
(13) Liu, J.; Guo, T. F.; Yang, Y. *J. Appl. Phys.* **2002**, *91*, 1595.
(14) Watanabe, J.; Harkness, B. R.; Sone, M.; Ichimura, H. *Macromolecules* **1994**, *27*, 507.
(15) Hsu, J. H.; Fann, W.; Tsao, P. H.; Chuang, K. R.; Chen, S. A. *J. Phys. Chem. A* **1999**, *103*, 2375.
(16) Chang, R.; Hsu, J. H.; Fann, W. S.; Yu, J.; Lin, S. H.; Lee, Y. Z.; Chen, S. A. *Chem. Phys. Lett.* **2000**, *317*, 153.
(17) Hsu, J. H.; Hayashi, M.; Lin, S. H.; Fann, W.; Rothberg, L. J.; Perng, G. Y.; Chen, S. A. *J. Phys. Chem. B* **2002**, *106*, 8582.
(18) Hsu, J. H.; Chang, R.; Lin, S. H.; Fann, W.; Perng, G. Y.; Chen, S. A. Manuscript submitted to *Phys. Rev. B*.
(19) Wudl, F. US Pat. No. 5189136, 1990; *Chem. Abstr.* **1993**, *118*, 255575p.
(20) Gieniewski, C.; Moore, R. S. *Macromolecules* **1970**, *3*, 97.
(21) Bush, T. E.; Scott, G. W. *J. Phys. Chem.* **1981**, *85*, 144.

MA035230N